Assessing the nonequilibrium of decaying turbulence with reversed initial fields

F. Liu (刘锋),[1,2] L. P. Lu (陆利蓬),[2] Wouter J. T. Bos,[3,*] and L. Fang (方乐)[1,†]

[1]*Laboratory of Mathematics and Physics, Ecole Centrale de Pékin, Beihang University, Beijing 100191, China*

[2]*National Key Laboratory of Science and Technology on Aero-Engine Aero-Thermodynamics, School of Energy and Power Engineering, Beihang University, Beijing 100191, China*

[3]*LMFA, CNRS, Ecole Centrale de Lyon–Université de Lyon, 69130 Ecully, France*

(Received 7 November 2018; published 8 August 2019)

Recently, it was observed that in nonequilibrium turbulent flows the normalized dissipation rate depends in a fairly universal way on the Reynolds number of the flow. To assess theoretical explanations of this observation, we consider here the nonequilibrium properties of freely decaying turbulence from initial conditions where the velocity field is reversed in every point in space. This test-case allows us to manipulate a turbulent flow differently from the usual way, where nonequilibrium is induced by modification of large-scale forcing mechanisms. It is shown that it is possible to obtain a different Reynolds-dependent scaling of the dissipation rate, which can be derived directly as a perturbation around the equilibrium state.

DOI: 10.1103/PhysRevFluids.4.084603

I. INTRODUCTION

Three-dimensional turbulent flows are generally far from statistical equilibrium [1,2]. Indeed, if turbulence is considered as a high-dimensional dynamical system, then statistical equilibrium would correspond to an equipartition of kinetic energy over Fourier-modes [3]. However, viscous dissipation rapidly removes energy from the modes with large wave number, such that turbulent systems are kept away from this equilibrium state. Consequently, to approach equilibrium, large-scale energy is transferred toward these smaller scales [4]. In the case of a slowly evolving large-scale flow structure, the small scales of a turbulent flow rapidly adapt to the energy input, and for a steady input, a statistical steady state will emerge, where dissipation is equal to production. It is this equilibrium transfer between large and small scales, a direct consequence of the inherent nonequilibrium of turbulence, which is an essential ingredient of a large number of statistical models and theories.

In such a steady state, small-scale dissipation ε is directly determined by the large scales, characterized by the integral length L and velocity U scales. This interdependence can be quantitatively represented by the expression

$$\varepsilon = C_\varepsilon \frac{U^3}{L}. \tag{1}$$

The proportionality constant, also called normalized dissipation rate, is then supposed to be independent of the Reynolds number, for a given flow at large Reynolds number.

*wouter.bos@ec-lyon.fr

†le.fang@zoho.com

Obviously, numerous situations can be thought of where the energy input is not steady, so that the equilibrium has not had a change to establish. Such nonequilibrium flows are the rule rather than an exception, and the inherent nonequilibrium of unsteady flows has recently received a considerable amount of attention, in particular the case of decaying grid-generated wind-tunnel turbulence [5–7]. Indeed, this case is the simplest experimental realization of nearly isotropic turbulence and is inherently unsteady, since in the reference frame moving with the mean velocity, the external energy input is zero.

In the studies on grid-generated turbulence some universality was observed in the nonequilibrium properties of the flow, not too far behind the grid [6,7]. The dissipation coefficient C_ε was there shown to be characterized by a functional dependence of the Reynolds number of the form

$$C_\varepsilon \sim \mathrm{Re}_I{}^m / \mathrm{Re}_L{}^n, \tag{2}$$

where Re_I and Re_L are a global Reynolds number (characterizing the initial conditions) and a local Reynolds number, respectively. The values of m and n were observed to be close to unity. A theoretical explanation was proposed recently [8] where it was shown that the value $m = n \approx 15/14$ can be derived analytically, using a first-order perturbation analysis of the energy flux around its equilibrium value ε_0. This derivation does not only concord with the experimental observations but also explains the observations in direct numerical simulations (DNSs) with a strongly fluctuating energy input [9]. A rival explanation exists, which links the nonequilibrium scaling to the coexistence of strong coherent structures with a less coherent background turbulence [10,11]. An attempt to represent this interplay between coherent structures and a background flow in the framework of a statistical closure was presented in Ref. [12]. A more complete description, modeling explicitly the interaction between the wakes behind the grid-bars and the turbulence [13], shows that the nonequilibrium scaling persists in the region where the kinetic energy of the grid-bar-wakes is comparable to the kinetic energy of the turbulent fluctuations.

In the DNSs and in grid-generated turbulence the production mechanism is a typical large-scale phenomenon. In the present investigation, to lend further support to the nonequilibrium explanation [8], we consider a case in which we can induce strong nonequilibrium in the small scales and where this nonequilibrium persists for some time. This case is time-reversed turbulence, where the sign of the velocity is reversed in every point in space.

II. THE NORMALIZED DISSIPATION IN NONEQUILIBRIUM TURBULENCE

We recall first rapidly the main ingredients in the derivation of the nonequilibrium scaling [8]. An important insight is the fact that, for slowly evolving large-scale flow, the imbalance is mainly reflected in the large scales of the flow, the small scales reacting, and adapting, rapidly to the changing energy input. The dynamic quantities k, L, ε are then all divided into an equilibrium value k_0, L_0, ε_0, corresponding to their values in a constant flux state, and the deviations from this state, $\tilde{k}, \tilde{L}, \tilde{\varepsilon}$. It was shown that when the energy input in a flow changes, it is L and k which deviate from their equilibrium values. Furthermore, it was shown that $\tilde{L}/L_0 \approx \frac{3}{7}\tilde{k}/k_0$, and $\tilde{\varepsilon}/\varepsilon_0 \approx 0$. Thereby, it was derived that

$$C_\varepsilon = C_{\varepsilon 0}\left(1 - \frac{15}{14}\frac{\tilde{k}}{k_0}\right) \tag{3}$$

and

$$\mathrm{Re}_\lambda = \mathrm{Re}_{\lambda 0}\left(1 + \frac{\tilde{k}}{k_0}\right), \tag{4}$$

with the definitions

$$C_{\varepsilon 0} = \left(\frac{3}{2}\right)^{3/2} \frac{\varepsilon_0 L_0}{k_0^{3/2}} \tag{5}$$

and

$$\mathrm{Re}_{\lambda 0} = \sqrt{\frac{20}{3}} \frac{k_0}{\sqrt{\nu \varepsilon_0}}. \tag{6}$$

Therefore, since for small x, $(1+\alpha x) \approx (1+x)^{\alpha}$, Eqs. (3) and (4) yield a Reynolds number dependence of the normalized dissipation rate close to the power law observed in the experiments and simulations,

$$\frac{C_\varepsilon}{C_{\varepsilon 0}} \approx \left(\frac{\mathrm{Re}_\lambda}{\mathrm{Re}_{\lambda 0}} \right)^{-\frac{15}{14}}. \tag{7}$$

Indeed, this power law is observed in the experiments or DNS for a change in Reynolds number of less than an octave, so that the linearization of the power law does not lead to an error of more than several percents. For instance, in Fig. 3 of the DNS study of Ref. [9] fluctuations around equilibrium states are shown for different Reynolds numbers. For each case individually, the ratio of maximum to minimum Reynolds number is of order two at most. Further implications of this analysis are that the Taylor-scale, defined by

$$\lambda = \sqrt{\frac{20}{3} \frac{k\nu}{\varepsilon}}, \tag{8}$$

compared to the integral scale will scale as [8]

$$\frac{L}{\lambda} \frac{\lambda_0}{L_0} \approx \left(\frac{\mathrm{Re}_\lambda}{\mathrm{Re}_{\lambda 0}} \right)^{-1/14}, \tag{9}$$

with λ_0 the Taylor scale in the equilibrium state. This expression is substantially different from equilibrium scaling,

$$\frac{L}{\lambda} \sim \mathrm{Re}_\lambda^1. \tag{10}$$

We stress again that it is the large-scale quantities L and k which are affected by nonequilibrium. But what happens if we do not act dominantly on the large scales, but directly and strongly alter the dissipation rate, without too much affecting the large scales? This seems experimentally very difficult to achieve. In simulations this is, however, easier, and for this we reconsider a test-case which we investigated in an earlier investigation [14], time-reversed turbulence. The thought-experiment in which the velocity is reversed in every point in space was already proposed by Orszag in his turbulence lectures [15], and since then it was considered by several authors in the context of large eddy simulation [16,17].

To explain the dynamics of time-reversed turbulence in some more detail, we write the equation for the kinetic energy spectrum. The energy spectrum $E(\kappa, t)$ is defined such that its integral over all wave numbers κ equals the kinetic energy,

$$\int E(\kappa, t) d\kappa = k(t). \tag{11}$$

As a function of time, the spectrum evolves as

$$\partial_t E(\kappa, t) = T(\kappa, t) - 2\nu\kappa^2 E(\kappa, t). \tag{12}$$

The quantity $T(\kappa, t)$ is the energy transfer. This transfer is associated to a triple-velocity correlation and represents the transfer between different scales or wave numbers κ. The dynamics of the Euler equations are invariant under the simultaneous transformation $\boldsymbol{u}$ to $-\boldsymbol{u}$, t to $-t$. Indeed, the term $\partial_t E(\kappa, t)$ changes sign when t is replaced by $-t$ and triple velocity correlations change sign when $\boldsymbol{u}$ is replaced by $-\boldsymbol{u}$. This means that if all velocities are reversed, then the flow will evolve backwards in time until the initial condition is reached. Indeed, the dissipation term $2\nu\kappa^2 E(\kappa, t)$ is not affected

by the reversal of $\boldsymbol{u}$, so that viscous effects will break the exact time-reversal. However, at the large scales where viscous effects are less important, the reversal of the velocity will lead to approximate time-reversed dynamics for some time. What we investigated previously, is how the dynamics change if either the whole flow, or a part is reversed, for Navier-Stokes turbulence. The relevance of this investigation was to investigate how a subgrid model should behave in the presence of strong and weak backscatter [14].

Other cases could be considered, for instance a low-pass filtered initial condition, or an initial field where only the dissipation scale is reversed. We have investigated several of these cases, but find the most interesting results for the reversed initial conditions. Indeed, in addition to a radical change in the dissipation rate dynamics, this case corresponds to a situation of very strong backscatter, affecting the energy-transfer of all the different scales of the turbulent flow. That this case leads to the most important change of the dynamics is due to the fact that in addition to changing the small scales, the large scales do not directly drain their energy toward the small scales, since the transfer is reversed. Therefore, the time-interval over which the flow is affected is longer than for a case where only the small scales are reversed or where their energy is set to zero. In the remainder of this work we will therefore focus on the case of reversed conditions for all scales and assess the nonequilibrium properties of such a flow.

III. NUMERICAL RESULTS

A. Numerical setup and parameters

DNS cases are performed by using a standard pseudospectral solver and a fourth-order Runge-Kutta time integration scheme, with a semi-implicit treatment of the viscous term. The computational domain has 512^3 grid points. All cases start from a freely decaying isotropic turbulence with the same random initial field in a $(4\pi)^3$ periodic cube [18], with a spectral energy distribution similar to the measured spectrum in the experimental work of Comte-Bellot and Corrsin [19].

Two distinct cases are considered: 'normal' freely decaying isotropic turbulence, indicated by "NN" using the same nomenclature as in Ref. [14] and a reversed case denominated "RR" corresponding to the same flow where the sign of the velocity in every point in space is reversed at a given time (denoted as $t = 0$. At this moment $\mathrm{Re}_\lambda \approx 110.9$, and $k_{\max}\eta = 1.12$). Numerical details are the same as Ref. [14], except that the cases here are recalculated with higher resolutions (512^3 instead of 256^3). The time values are normalized by using the turn-over time at the moment of reversal $T = \sqrt{3/2}(k/\varepsilon)$, where k is the kinetic energy, and ε is the turbulent energy dissipation rate.

B. A new dissipation scaling

In our simulations the flow develops from random initial conditions. The turbulence will decay, after a certain time, as a power law, with $k/\epsilon \sim t$. This power-law decay region is situated, in time, well beyond the transient nonequilibrium region where relation Eq. (7) is valid and in this self-similar decaying regime the normalized dissipation is expected to be roughly constant, if $\mathrm{Re}_\lambda \gg 100$. The fact that a constant value for C_ε can be observed in freely decaying turbulence with a value different from its steady state value was already explained in previous work [20], using the notion of a Reynolds-number-independent-imbalance between large and small scales. Note that our Reynolds number is not large enough to be completely in this asymptotic regime. Direct numerical simulations [21] suggest that the cross-over to a Reynolds number independent value of the normalized dissipation takes place in the range $100 < \mathrm{Re}_\lambda < 200$. In our investigation the time-instant $t = 0$ corresponds to the time at which the flow is reversed and this time-instant is chosen well beyond the transient region, within this self-similar decay regime.

In Fig. 1(a) we plot the values of C_ε and Re_λ during the simulations. The direction of time is indicated by arrows. For the NN case (red line) C_ε is not completely constant but slowly

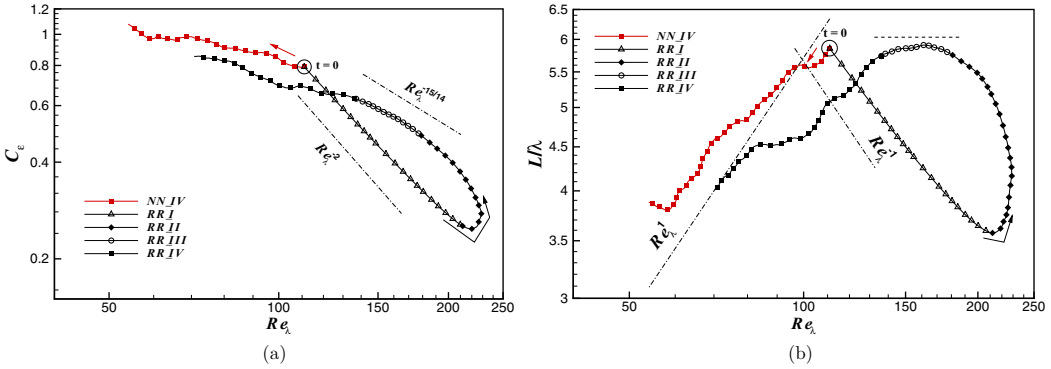

FIG. 1. (a) Relation between dissipation coefficient C_ε and Reynolds number Re_λ in different evolution stages. Stages are marked as *I*, *II*, *III*, and *IV*, respectively. (b) Relation between L/λ and Reynolds number Re_λ in different evolution stages. Stages are marked as *I*, *II*, *III*, and *IV*, respectively. The dash-dotted lines corresponds to $L/\lambda \propto \mathrm{Re}_\lambda$, and $L/\lambda \propto \mathrm{Re}_\lambda^{-1}$. Arrows indicate the time directions.

increasing in time, which can be explained when taking into account the finite value of the Reynolds number [20].

The complementary scaling for L/λ as a function of Re_λ is shown in Fig. 1(b), showing that for the NN case (red line) L/λ is approximately proportional to Re_λ, as predicted by traditional Kolmogorov theories [22]. Note that at the Reynolds numbers at which our simulations are carried out this relation is expected to be valid only to some approximation.

The behavior of the dissipation rate scaling for the reversed case is radically different. To discuss the behavior, we divide the time evolution into four qualitatively different temporal stages.

(*I*) Time interval $[0 < t/T < 0.2]$. In the beginning, a large and rapid variation of the dissipation coefficient is observed, $C_\varepsilon \propto \mathrm{Re}_\lambda^{-2}$ (empty triangles). Furthermore, during this interval $L/\lambda \propto \mathrm{Re}_\lambda^{-1}$.

(*II*) Time interval $[0.2 \leqslant t/T < 1.5]$. A transition stage is observed (filled diamonds).

(*III*) Time interval $[1.5 \leqslant t/T < 2.4]$. The graphs show nonequilibrium scaling in agreement with existing observations in grid-generated turbulence (empty circles). This corresponds to approximately constant values of L/λ while the $C_\varepsilon \propto \mathrm{Re}_\lambda^{-15/14}$.

(*IV*) Freely decaying turbulence with self-similar scaling is observed at longer times (filled squares), similar to the NN case. This corresponds to $L/\lambda \propto \mathrm{Re}_\lambda$ [see Fig. 1(b)] and slowly increasing values of C_ε with time [see Fig. 1(a)].

Probably the most intriguing observation is the very clear power-law scaling for C_ε and L/λ at short times in stage *I*. Moreover, this scaling is radically different from the scaling behavior in recent experiments and simulations. We will explain this observation in Sec. IV A.

C. Time-evolution of the integral quantities

As stressed in Sec. II, the nonequilibrium scaling observed in grid-generated turbulence is related to the deviations of the large scales, characterized by k and L, from an equilibrium state. Changing the sign of the velocity changes the sign of the energy transfer, an effect which is not instantaneously felt by the large scales, but which radically changes the small-scale dynamics. For instance, the value of the longitudinal velocity gradient skewness,

$$S_k = \frac{\langle(\partial u_1/\partial x_1)^3\rangle}{\langle(\partial u_1/\partial x_1)^2\rangle^{3/2}}, \tag{13}$$

changes its sign [Fig. 2(a)], which illustrates that the small scales are immediately affected, in particular the sign of the energy transfer, which is directly related to S_k. From Fig. 2(b) it is shown

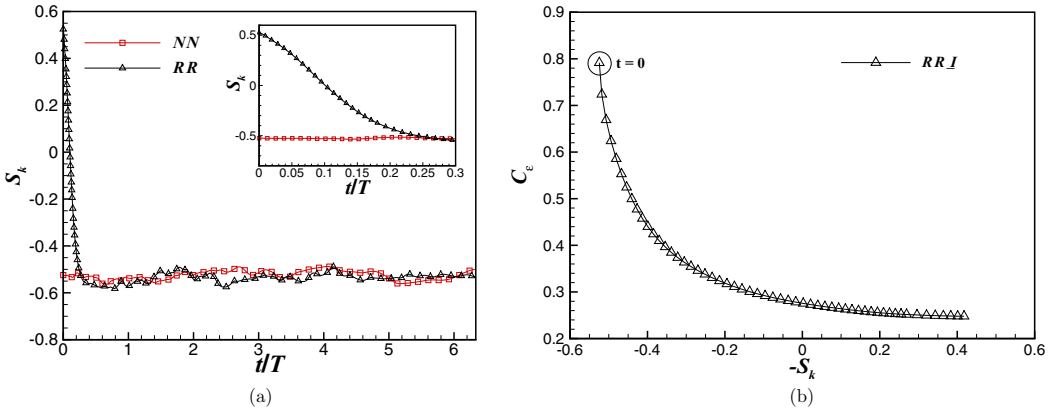

FIG. 2. (a) Temporal evolution of the skewness of longitudinal velocity derivative S_k. The subfigure is the zoom of stage *I*. (b) Variation of C_ε with S_k in stage *I*.

that the value of S_k is also clearly correlated with the value of C_ε in stage *I*, which qualitatively supports the conclusion of Ref. [23], that S_k might be considered as a sensitive indicator of nonequilibrium. However, in Fig. 4(a) of Ref. [23] they are positively correlated, differing from Fig. 2(b). This can be understood since the numerator of S_k is an odd moment which changes sign with reversed velocity field in short time, but C_ε does not change sign. This shows that the positive correlation between S_k and C_ε, observed in Fig. 4(a) of Ref. [23], is not a universal feature of nonequilibrium turbulence.

The reversal of the velocity does not change the sign of k, ε and L, which are all strictly positive quantities. These three quantities, together with C_ε are shown as a function of time in Fig. 3. In particular, the insets of these figures, zooming on the initial time interval, are interesting. These zooms clearly show that it is the dissipation which is most strongly affected in this flow. Indeed, since the dissipation scales are no longer supplied with new energy from the large scales, which is flowing in backwards direction, and since the viscous friction will continue to remove the energy from the same small scales, the dissipation drops rapidly. Note that from Fig. 3(b) it is observed that L is always much smaller than the box size 4π (qualitatively, $0.11 < L/4\pi < 0.25$, consistent with setups in literature such as Refs. [24–27], though in some literature [28] it was argued that finite size effect remains).

A diminished dissipation also corresponds to a slower-decaying kinetic energy, compared to the unmodified case, which is clearly observed. Furthermore the inverse energy cascade will for short times generate a larger integral correlation scale. However, this build up is on a slower timescale than the evolution of the dissipation.

To summarize, the dissipation evolves at short times much faster than the large-scale quantities k and L.

IV. ORIGIN OF THE NEW NONEQUILIBRIUM SCALING

A. Derivation of the scaling

The newly observed scaling of C_ε can be readily derived, using the observations in the previous section. Indeed at short times it is the dissipation which evolves most rapidly. We therefore consider an equilibrium state, represented by the quantities k_0, L_0, and ε_0. In the derivation of the nonequilibrium scaling of Ref. [8], the quantities k and L deviated from their equilibrium state. In the present case, as can be concluded from the observations in the previous section, it is the dissipation ε which is affected. Therefore, we replace in the expression for the dissipation coefficient

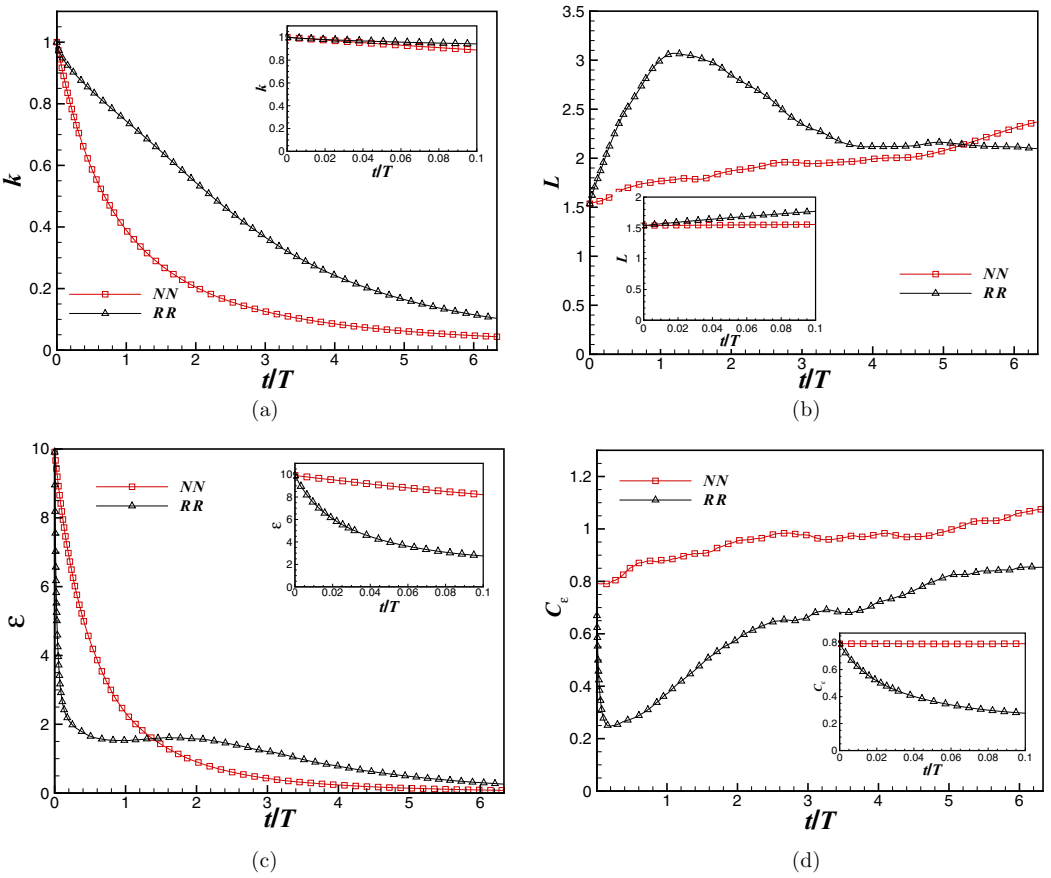

FIG. 3. Temporal evolution of (a) the kinetic energy k, (b) the integral scale L, (c) the turbulent energy dissipation rate ε, and (d) the dissipation coefficient C_ε. Insert: short-time evolution of each statistic.

the lengthscale and kinetic energy by their equilibrium values, and we let ε be a function of time,

$$C_\varepsilon(t) = \frac{\varepsilon(t) L_0}{(2k_0/3)^{3/2}}, \tag{14}$$

while the Reynolds number becomes

$$\mathrm{Re}_\lambda(t) = \sqrt{20/3}\frac{k_0}{\sqrt{\varepsilon(t)\nu}}. \tag{15}$$

The whole time-dependence will be driven by the only strongly changing quantity, $\varepsilon(t)$. Combining the above two equations, eliminating the time-dependent parameter ε, we have immediately

$$C_\varepsilon = \sqrt{150}\frac{k_0^{1/2} L_0}{\nu}\mathrm{Re}_\lambda^{-2}. \tag{16}$$

This shows thus that if we change the small, rapidly adapting scales, keeping the large scales approximately constant, then the time variation of C_ε as a function of Re_λ will become inversely quadratic $C_\varepsilon \sim \mathrm{Re}_\lambda^{-2}$ instead of relation Eq. (7), $\sim \mathrm{Re}_\lambda^{-15/14}$. Furthermore, measuring the Reynolds

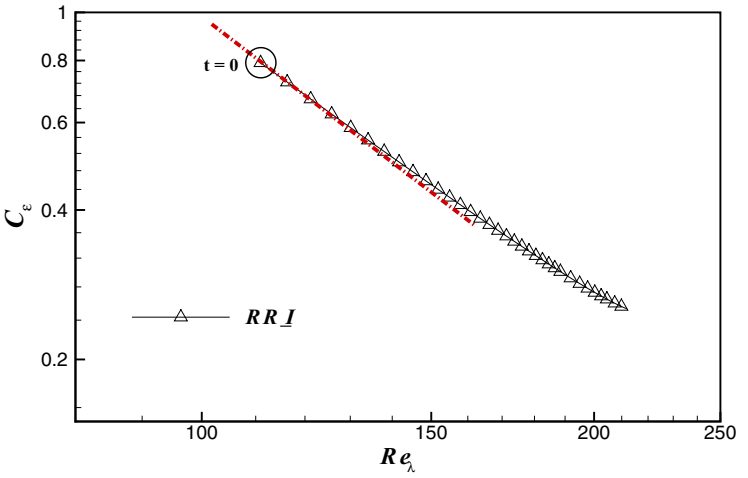

FIG. 4. Dissipation coefficient C_ε against Reynolds number Re_λ in stage *I*. The dash-dotted line represents the relation in Eq. (16).

number dependence of the lengthscale ration L/λ, from Eq. (16), we have immediately

$$\frac{L}{\lambda} = C_\varepsilon \mathrm{Re}_\lambda \sim \mathrm{Re}_\lambda^{-1}, \tag{17}$$

as observed in Fig. 1(b).

To further illustrate the validity of the above arguments we show in Fig. 4 the comparison of Eq. (16) with the numerical simulation. Indeed, it is not only the power-law exponent which is correctly predicted, but it is the full expression including the prefactor which collapses perfectly with the data at short times.

B. A further look at the nonequilibrium

We have thus understood from the observations that the nonequilibrium scaling in time-reversed turbulence is directly associated with the rapid evolution of the dissipation scales. To this end we have assessed the time-evolution of the integral quantities k, L, and ε. In this section we will further scrutinize the nonequilibrium properties of the flow, scale-wise. For this we evaluate the wave number dependence of the imbalance.

The energy spectrum and its evolution were introduced in Eqs. (11) and (12). The energy transfer is a redistributive term, and its integral over wave numbers is zero,

$$\int T(\kappa, t) d\kappa = 0. \tag{18}$$

Its integral from 0 to a certain wave number κ_c represents the flux of energy from smaller toward larger wave numbers than κ_c,

$$\Pi(\kappa_c, t) = \int_0^{\kappa_c} T(\kappa, t) d\kappa, \tag{19}$$

furthermore, we can define the partial dissipation,

$$\varepsilon^>(\kappa_c, t) = \int_{\kappa_c}^{\infty} 2\nu\kappa^2 E(\kappa, t) d\kappa. \tag{20}$$

The difference between Π and $\varepsilon^>$ is a direct measure for the imbalance of the flow.

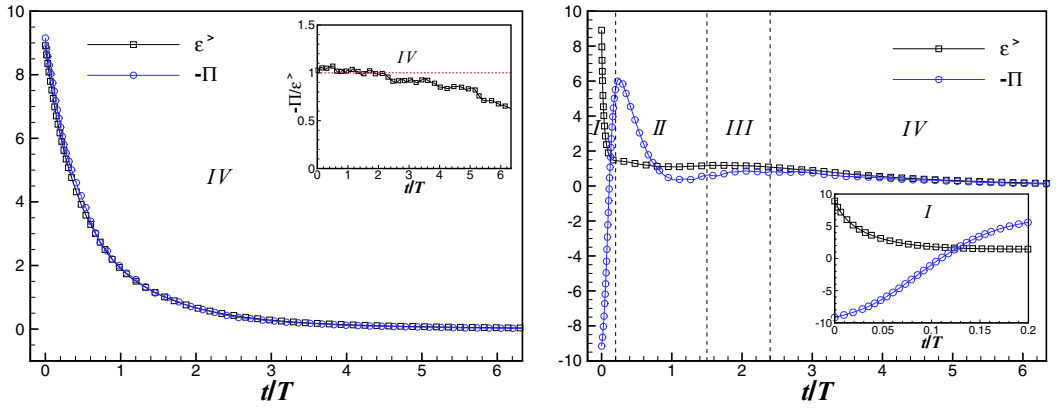

FIG. 5. Comparison between energy flux $-\Pi(\kappa_c, t)$ and dissipation $\varepsilon^>(\kappa_c, t)$, with κ_c fixed and its value is shown in Fig. 6. (a) NN, the inset shows $-\Pi/\varepsilon^>$; (b) RR, the inset shows a zoom view on the early evolution of the quantities.

In Fig. 5(a), it is clearly observed that the normal case can be considered to be close to equilibrium, since $\Pi \approx -\varepsilon^>$ during the whole time-evolution of the flow. Note that we have chosen $\kappa_c = 0.12\kappa\eta_0$, where η_0 is the kolmogorov scale at the time of reversal. This location corresponds to the maximum of the flux Π at $t = 0$. In Fig. 6(a), no asymptotic scaling $[E(\kappa) \propto \kappa^{-5/3}]$ is observed, as is usual in moderate Reynolds number, decaying turbulence [29]. By contrast, in the RR case [Fig. 5(b)] the equilibrium $\Pi \approx -\varepsilon^>$ is heavily perturbed. At the time of reversal, the flux takes the opposite sign. However, the value of $-\Pi$ rapidly increases, and an overshoot is observed, reaching a peak largely superior to $\varepsilon^>$ at a time instant that we will call $\Theta(\kappa)$. The time $t = \Theta(\kappa)$ is approximately the end of stage *I* when κ_c is close to the bottleneck region (see Fig. 6).

This timescale, corresponding to the time it takes from the time of reversal until the moment that the transfer flux reaches its peak-value, measures the reaction time of the turbulence up to a scale κ_c to react to the nonequilibrium. Figure 7 shows $-\Pi$ at different times, in which we can observe that the timescale depends on the wave number in the RR case: $-\Pi$ evolves faster toward equilibrium at higher wave numbers. This timescale is then quantitatively calculated as follows. In Fig. 8(a) the early time evolution of Π is shown for different values of the wave number κ_c. It is observed

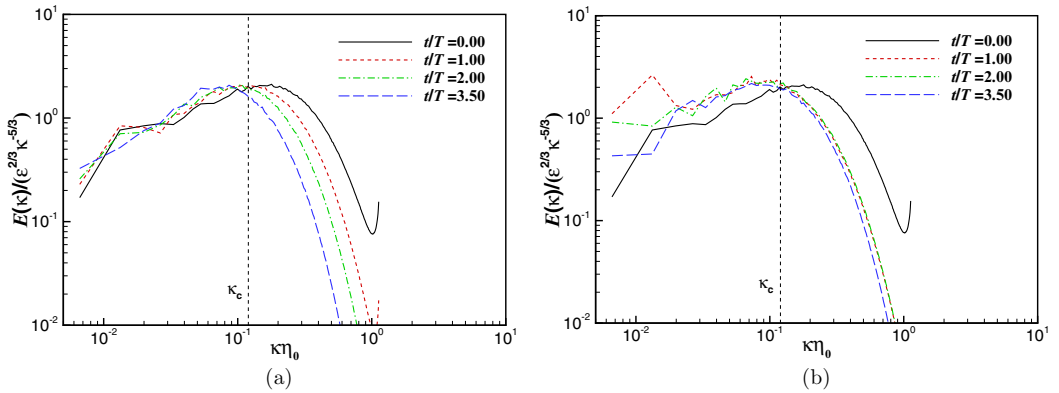

FIG. 6. Compensated energy spectra for (a) NN case and (b) RR case, respectively. The vertical dashed lines indicate the location of κ_c used in Fig. 5.

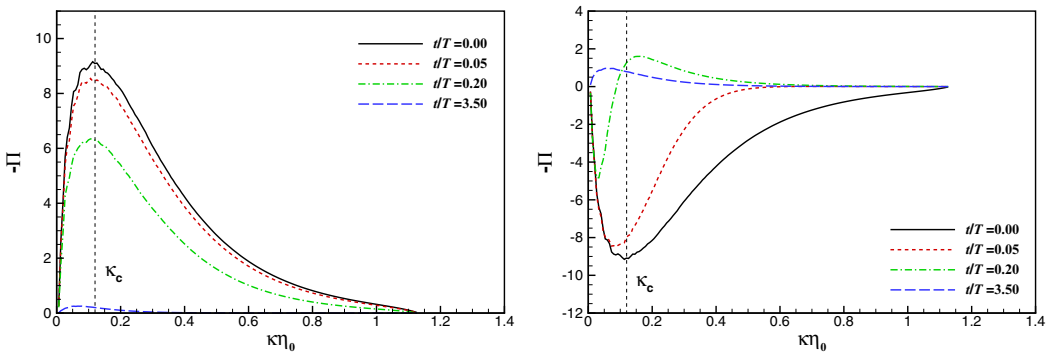

FIG. 7. Energy flux $-\Pi(\kappa, t)$ at different times. (a) NN; (b) RR. The vertical dashed lines indicate the location of κ_c used in Fig. 5.

that when the value of κ_c increases (moving toward the dissipative range), the reaction time $\Theta(\kappa)$, decreases. Indeed, qualitatively this shows that the small scales react faster than the large scales. In Fig. 8(b) the value of $\Theta(\kappa)$ is plotted as a function of κ. It is observed that the reaction time in the inertial range is proportional to $\kappa^{-2/3}$, in agreement with classical scaling arguments [22]. Indeed, what we measure is the time it takes for a given scale to adapt back to the usual energy transfer direction. This timescale is expected to be of the order of the typical lifetime of the eddy associated with wave number κ. This timescale is, in the absence of viscous effects, mainly determined by the cumulative straining induced by larger eddies. A typical estimate of this time $\tau(\kappa)$ is

$$\tau(\kappa) \sim \left[\int_0^\kappa p^2 E(p) dp\right]^{-1/2}. \tag{21}$$

Since this straining time is a function of the energy spectrum, and not of the transfer, its estimate should give close to classical scaling for our reversed flow, since the energy spectrum is not directly affected by the reversal. For a spectrum proportional to $\kappa^{-5/3}$, $\tau(\kappa)$ should scale proportional to $\kappa^{-2/3}$. In the present case, there is no $\kappa^{-5/3}$ range in the energy spectrum due to the finite value

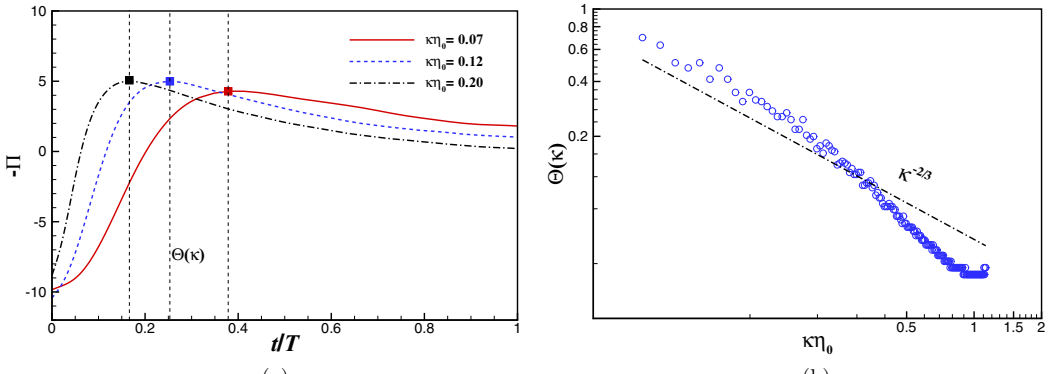

FIG. 8. (a) Temporal evolution of the energy flux $-\Pi(\kappa, t)$ at fixed wave numbers. The filled squares denote the maximum value of $\Pi(\kappa, t)$, defining the time $t = \Theta(\kappa)$. (b) The relationship between the characteristic time $\Theta(\kappa)$ and the wave number κ in reversed turbulence. The dash-dotted line indicates a power-law behavior proportional to $\kappa^{-2/3}$. The Kolmogorov scale $\eta_0 := \eta(t = 0)$ is used for normalization.

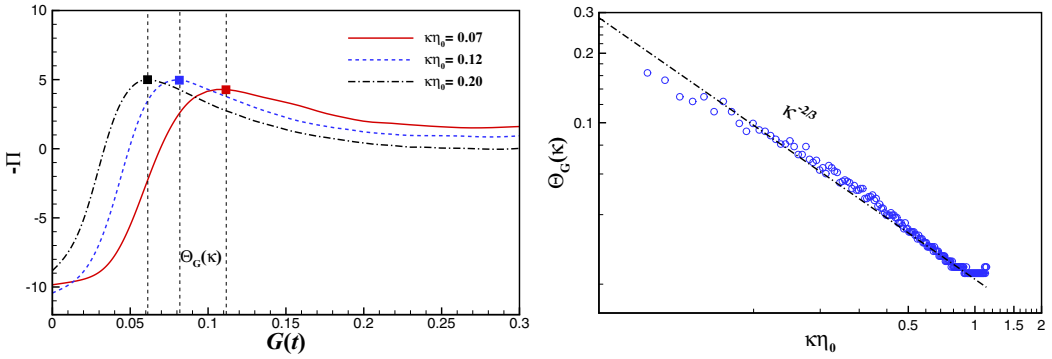

FIG. 9. (a) Temporal evolution of the energy flux $-\Pi(\kappa, t)$ at fixed wave numbers. The filled squares denote the maximum value of $\Pi(\kappa, t)$, defining the time $G(t) = \Theta_G(\kappa)$. (b) The relationship between the characteristic time $\Theta_G(\kappa)$ and the wave number κ in reversed turbulence. The dash-dotted line indicates a power-law behavior proportional to $\kappa^{-2/3}$. The Kolmogorov scale $\eta_0 := \eta(t = 0)$ is used for normalization.

of the Reynolds number, but a $\kappa^{-2/3}$ scaling is approximately observed for the nonequilibrium timescale. This rather puzzling observation, that the nonequilibrium timescale satisfies classical scaling whereas the energy-spectrum does not, might be related to a different dependence on nonlocal interactions of the two quantities. Further investigation using triadic closures [30] might shed further light on this.

We can also define the localized nondimentional time $G(t) := \int_0^t T(s)^{-1} ds$, where $T(s)$ is the eddy turnover time at time s, and then define the timescale at wave number κ [9] [see Fig. 9(a)], denoted as $\Theta_G(\kappa)$. It is shown in Fig. 9(b) that the $\kappa^{-2/3}$ law is even better satisfied by comparing to Fig. 8(b), which supports the use of $G(t)$ in the nondimensionalization of nonequilibrium turbulence [9].

These observations show that the dynamics of the dissipation in the reversed flows is radically affected, in particular since the reversed transfer depletes the dissipation scales from their energy. The time it takes for structures in a flow with a length scale associated with the wave number κ, to return from their backwards energy transfer toward their conventional forward transfer, scales as $\kappa^{-2/3}$. Since the reversal does not change the variance of the velocity, the energy spectrum is unchanged at the time of reversal. The scaling of the imbalance is thus determined by the equilibrium state. Indeed, this was also the rationale of the derivation of the nonequilibrium scaling [8], where the imbalance was determined as a perturbation around the equilibrium state.

V. CONCLUSIONS

We have explored the nonequilibrium of time-reversed turbulence. Indeed, this type of flow, where the velocity is reversed at every point in space can be considered to be one of the most extreme cases of nonequilibrium turbulence. It is observed that the recently discovered nonequilibrium scaling of the normalized dissipation rate [7,8] is not observed at the time of reversal. Instead we show that during the time interval, in which the reversed flow reorganizes to restore its energy cascade, a new dissipation scaling is observed, where $C_\varepsilon \sim \mathrm{Re}_\lambda^{-2}$, which corresponds to the nonequilibrium transient in which the dissipation evolves rapidly, independent from the large-scale quantities L and k.

The derivation in Ref. [8] shows that in grid turbulence, or decaying box-turbulence, the dissipation scaling Eq. (7) can be obtained by a perturbation expansion around an equilibrium flux of energy, assuming weak disequilibrium. In the present case this derivation is not valid since the flux of energy is completely reversed, which corresponds to a case where the size of the perturbation

is twice the equilibrium flux. We can therefore not use the same perturbation around an equilibrium flux. However, when we consider the energy spectrum and the large scales to be frozen, and assume that only the dissipation evolves, the exact scaling $C_\varepsilon \sim \mathrm{Re}_\lambda^{-2}$ can be derived.

We further show that the time it takes for a structure with a typical wave number to restore its equilibrium transfer scales as $\kappa^{-2/3}$. At later times, when the dissipation is again slaved to the large-scale dynamics, the behavior of C_ε evolves back to the behavior observed in preceding simulations and experiments.

Both the present investigation and Ref. [8] show that imbalance in turbulence can often be considered a perturbation around an equilibrium state. In the present case, it is a perturbation of the dissipation scales, whereas in most nonequilibrium flows the imbalance reflects a deviation of the large energy-containing scales from their equilibrium value.

The case of time-reversed turbulence can be considered to be an extreme example of energy backscatter. It can therefore be expected that in more complex flows, during strong backscatter events, localized in space and or time, the dissipation rate behaves as in the present investigation. For example, S_k can be positive in the internal flow of compressors (see Fig. 13 of Ref. [31]), indicating a strong local backscatter. Taking into account such events in engineering turbulence models might turn out an interesting direction for future research.

ACKNOWLEDGMENTS

We are grateful to Y. Zhu and R. Rubinstein for the discussions. This work is supported by the National Natural Science Foundation of China (Grants No. 11572025, No. 11772032, and No. 51420105008).

[1] W. Wu, F. Zhang, and J. Wang, Potential landscape and flux field theory for turbulence and nonequilibrium fluid systems, Ann. Phys. **389**, 63 (2018).
[2] K. R. Sreenivasan and R. A. Antonia, The phenomenology of small-scale turbulence, Annu. Rev. Fluid Mech. **29**, 435 (1997).
[3] T. D. Lee, On some statistical properties of hydrodynamical and magneto-hydrodynamical fields, Q. Appl. Math. **10**, 69 (1952).
[4] A. N. Kolmogorov, The local structure of turbulence in incompressible viscous fluid for very large Reynolds number, Proc. Math. Phys. Sci. **30**, 301 (1941).
[5] R. E. Seoud and J. C. Vassilicos, Dissipation and decay of fractal-generated turbulence, Phys. Fluids **19**, 105108 (2007).
[6] P. C. Valente and J. C. Vassilicos, Universal Dissipation Scaling for Nonequilibrium Turbulence, Phys. Rev. Lett. **108**, 214503 (2012).
[7] J. C. Vassilicos, Dissipation in turbulent flows, Annu. Rev. Fluid Mech. **47**, 95 (2015).
[8] W. J. T. Bos and R. Rubinstein, Dissipation in unsteady turbulence, Phys. Rev. Fluids **2**, 022601 (2017).
[9] S. Goto and J. C. Vassilicos, Energy dissipation and flux laws for unsteady turbulence, Phys. Lett. A **379**, 1144 (2015).
[10] S. Goto and J. C. Vassilicos, Unsteady turbulence cascades, Phys. Rev. E **94**, 053108 (2016).
[11] F. A. Portela, G. Papadakis, and J. C. Vassilicos, Turbulence dissipation and the role of coherent structures in the near wake of a square prism, Phys. Rev. Fluids **3**, 124609 (2018).
[12] M. Meldi and P. Sagaut, Investigation of anomalous very fast decay regimes in homogeneous isotropic turbulence, J. Turbulence **19**, 390 (2018).
[13] W. J. T. Bos, Grid turbulence near the grid, https://hal.archives-ouvertes.fr/hal-02063500 (2019).
[14] L. Fang, W. J. T. Bos, L. Shao, and J.-P. Bertoglio, Time-reversibility of Navier-Stokes turbulence and its implication for subgrid scale models, J. Turbulence **13**, N3 (2012).

[15] S. A. Orszag, Lectures on the statistical theory of turbulence, in *Fluid Dynamics, Les Houches Summer School of Theoretical Physics*, edited by R. Balian and J.-L. Peube (Gordon and Breach, New York, 1974).
[16] D. Carati, G. S. Winckelmans, and H. Jeanmart, On the modeling of subgrid-scale and filtered-scale stress tensors in large-eddy simulation, J. Fluid Mech. **441**, 119 (2001).
[17] L. Fang, Y. Zhu, Y. W. Liu, and L. P. Lu, Spectral nonequilibrium property in homogeneous isotropic turbulence and its implication in subgrid-scale modeling, Phys. Lett. A **379**, 2331 (2015).
[18] R. S. Rogallo, *Numerical Experiments in Homogeneous Turbulence* (NASA, Washington, D.C., 1981).
[19] G. Comte-Bellot and S. Corrsin, The use of contraction to improve the isotropy of grid generated turbulence, J. Fluid Mech. **25**, 657 (1966).
[20] W. J. T. Bos, L. Shao, and J. P. Bertoglio, Spectral imbalance and the normalized dissipation rate of turbulence, Phys. Fluids **19**, 045101 (2007).
[21] Y. Kaneda, T. Ishihara, M. Yokokawa, K. Itakura, and A. Uno, Energy dissipation rate and energy spectrum in high resolution direct numerical simulations of turbulence in a periodic box, Phys. Fluids **15**, L21 (2003).
[22] H. Tennekes and J. L. Lumley, *A First Course in Turbulence* (MIT press, Cambridge, MA, 1972).
[23] R. J. Hearst and P. Lavoie, Velocity derivative skewness in fractal-generated, nonequilibrium grid turbulence, Phys. Fluids **27**, 071701 (2015).
[24] T. Watanabe and T. Gotoh, Statistics of a passive scalar in homogeneous turbulence, New J. Phys. **6**, 40 (2004).
[25] Y. Li, E. Perlman, M. Wan, Y. Yang, C. Meneveau, R. Burns, S. Chen, A. Szalay, and G. Eyink, A public turbulence database cluster and applications to study Lagrangian evolution of velocity increments in turbulence, J. Turbulence **9**, N31 (2008).
[26] R. Samtaney, D. I. Pullin, and B. Kosovic, Direct numerical simulation of decaying compressible turbulence and shocklet statistics, Phys. Fluids **13**, 1415 (2001).
[27] L. Fang, Background scalar-level anisotropy caused by low-wave-number truncation in turbulent flows, Phys. Rev. E **95**, 033102 (2017).
[28] B. Thornber, Impact of domain size and statistical errors in simulations of homogeneous decaying turbulence and the Richtmyer-Meshkov instability, Phys. Fluids **28**, 045106 (2016).
[29] L. Mydlarski and Z. Warhaft, Passive scalar statistics in high-Peclet-number grid turbulence, J. Fluid Mech. **358**, 135 (1998).
[30] M. Lesieur, *Turbulence in Fluids* (Kluwer Academic, Dordrecht, 1997).
[31] L. Fang, H.-K. Zhao, L.-P. Lu, Y.-W. Liu, and H. Yan, Quantitative description of nonequilibrium turbulent phenomena in compressors, Aerosp. Sci. Tech. **71**, 78 (2017).